Liquid Crystals
Publication details, including instructions for authors and subscription information:
http://www.informaworld.com/smpp/title~content=t713926090

Electro-optical properties of conic cylindrical-cavities liquid crystal displays

Bau-Jy Liang; Shu-Hsia Chen; Chi-Ray Wu

Online publication date: 11 November 2010

To cite this Article Liang, Bau-Jy , Chen, Shu-Hsia and Wu, Chi-Ray(2002) 'Electro-optical properties of conic cylindrical-cavities liquid crystal displays', Liquid Crystals, 29: 5, 697 — 706
To link to this Article: DOI: 10.1080/02678290210127788
URL: http://dx.doi.org/10.1080/02678290210127788

LIQUID CRYSTALS, 2002, VOL. 29, NO. 5, 697–706

Electro-optical properties of conic cylindrical-cavities liquid crystal displays

BAU-JY LIANG*
Department of Electronic Engineering, Feng Chia University, Taichung, Taiwan, ROC

SHU-HSIA CHEN and CHI-RAY WU
Institute of Electro-Optical Engineering, National Chiao Tung University, Hsinchu, Taiwan, ROC

(*Received 21 March 2000; in final form 12 November 2001; accepted 17 December 2001*)

Experimental results have shown that the conic cavities in conic closed-cavity liquid crystal displays (conic CCLCDs) can give a wide viewing angle and grey levels without grey-scale inversion. The purpose of this paper is to extend investigations of conic CCLCDs. In experiments, we describe in detail the fabrication process, microscopic observations and optical measurements for conic CCLCDs. The simulation of director distribution will be based on the tensor form formulation of the free energy density. The differential equations satisfied by the steady-state director distribution are derived from this form of free energy and are solved in conjunction with Poisson's equation. The simulation of the optical propagation and the calculation of the optical transmittance will be based on the extended Jones matrix method. We show by simulation that a normal umbilical structure is the final stable state and that indeed conic CCLCDs can have a wide viewing angle and grey scale without grey-scale inversion. The theoretical results are compared with the experimental results. Transmittance, contrast ratio and viewing angle with various parameters of the LC are measured. Improved iso-contrast contours of the conic CCLCD with a *c*-plate compensator are also shown. Finally, we have also compared the electro-optical performance and the off axis colour-shift of the CCLCD, the 4-domain VAN device and the 4-domain twist-VAN device.

1. Introduction

Over the past years, liquid crystal displays (LCDs) have become widely used in applications such as laptop computer displays, monitors, and televisions. Even large screen applications are expected. The image quality of the LCDs has also been improved, and their resolution has become finer. Wide viewing angle, contrast ratio and no grey-scale inversion are favourable properties that make them an attractive choice for transmission LCDs. Recently, various methods for obtaining wide viewing angle LCDs have been proposed. These methods [1–4] used the domain-divided mode, in-plane-switching mode, vertical alignment mode and axially symmetric aligned microcell mode, as well as other optical compensation-film methods. Retardation film compensation improves the on–off electro-optical performance, but does not solve the grey scale problem. The four-domain vertical alignment nematic (4-D VAN) LCD and four-domain twisted vertical alignment nematic (4-D twisted VAN) LCD of these inversions also have a wide viewing angle. [5, 6] The conic CCLCD [7–9] is verified as possessing a wide viewing angle and no grey-scale inversion characteristics, as first reported by the author's research group. Due to the cylindrical axially symmetric properties, the conic CCLCD gives an excellent optical performance over a $\pm 70^\circ$ viewing angle in both the horizontal and vertical directions, under the condition of no grey-scale inversion.

As LCDs become more sophisticated, computer simulation likewise becomes more and more important. Simulation tools help in understanding the behaviour of the director and the optics of LCDs, and also in designing LCDs. To calculate a director configuration, it is necessary to express the free energy of the system. In the equilibrium state of the director with constant potential, the Gibbs free energy is minimized. The Gibbs free energy has elastic terms associated with the deformation of the director and external field terms. The electric field induced director field transition of a nematic liquid crystal in a closed conical cavity has been reported [10, 11]. The normal umbilic (NU) structure, twisted umbilic (TU) structure, normal hyperbolic (NH) point

*Author for correspondence; e-mail: bjliang@fcu.edu.tw

Liquid Crystals ISSN 0267-8292 print/ISSN 1366-5855 online © 2002 Taylor & Francis Ltd
http://www.tandf.co.uk/journals
DOI: 10.1080/02678290210127788

structure with a disclination ring, twisted hyperbolic (TH) point structure with a disclination ring, and normal Poincare (NP) structure are found to be stable in electric field-induced transitions. In this case, the configuration transition will not appear in the calculating process because the disclination position and form are fixed under the Frank–Oseen vector representation. The stable structure is determined by comparing the total energy of each structure under different applied voltages. The calculating sequences are very heavy and complicated. In the vector representation, the discretized free energy expression gives different free energies for **n** and $-\mathbf{n}$. In real nematics, however, **n** and $-\mathbf{n}$ are equivalent and should give the same torque and the same free energy. When the angle between two neighbouring discretized directors is greater than 90°, the torque is exerted between the two arrows, if the vector representation is used, rather than between the arrow and the tail, which make an angle less than 90°. The Landau–de Gennes Q tensor representation [12, 13] of the elastic free energy solves this problem. The Q tensor representation always incorporates the multiplication of two **n**s. By using the Q tensor representation, the disclination position and form may be changed, and director configurations can be more precisely calculated.

In this paper, we extend our preliminary investigation of the conic CCLCD and give some more detailed results and discussion. We will review the detailed fabrication processes and the experimental methods for conic CCLCDs in § 2. In § 3 the master equations for calculation are derived. Once the director field is obtained, the electro-optical properties can be calculated by the extended Jones matrix method [14]. In § 4 we give results about the stable structure in conic CCLCDs and the optical characteristics of CCLCDs, comparing also the results from simulation and from measurement. Also, the dependence of transmittance and contrast ratio on the optical parameters has been studied, and we demonstrate improved iso-contrast contours of the conic CCLCD with a *c*-plate compensator. The transmission versus voltage characteristics at normal incidence and off-axis colour shift of 4-D VAN, 4-D twisted VAN and CCLCDs are also compared. Finally, we give our conclusions in § 5.

2. Experimental

2.1. *Sample preparation*

The conic CCLCD was fabricated by filling the LC into conic cylindrical cavities as shown in figure 1 (*a*). These cavities are prepared by the techniques of semiconductor manufacture, so that their geometry and position can be very well controlled. The fabrication process for the conic CCLCD includes the following.

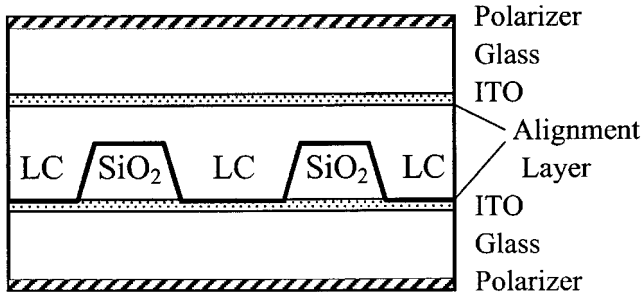

Figure 1. Schematic of the conic CCLCD.

2.1.1. *Fabrication of the cavities-glass plate*

An indium tin oxide (ITO)-coated glass plate was used as substrate. It is necessary to clean the substrates to avoid lines and defects on the surfaces. A layer of silicon dioxide (SiO_2) was grown about 3 μm thick on the substrate by plasma enhanced chemical vapour deposition. A mask having circles with both diameter and interval distances about 90 μm was made for the photolithography processes. The exposed substrate was coated with positive photoresist and then the pattern transformation was made from mask to SiO_2 layer. The exposed regions of positive photoresist layer were dissolved in a developing solution, and the circular hole pattern was left on the photoresist layer. The Buffered Oxide Etching (BOE) solution is suitable for etching the SiO_2 layer, but not for etching the ITO layer. After BOE had etched out the conic-cylindrical holes completely in the SiO_2 layer, the photoresist was removed from the top of the SiO_2 layer. Because we used wet etching processes that have an almost isotropic etching rate in the SiO_2 layer, the profiles of the etched holes resemble conical bowls.

2.1.2. *Coating with surfactant*

The conic CCLCD has two glass plates: one is the cavities-glass plate and the other is an even-glass plate coated with ITO. Before coating surfacant on the surface, cleaning processes for the plates are needed to ensure the quality of the alignment of the LC in the closed cavities. A perpendicular alignment of the LC director on the cavity walls was achieved by coating DMOAP (*N*,*N*-dimethyl-*N*-octadecyl-3-am inopropyltrimetho xysilyl chloride) on both the even-glass plate and the cavities-glass plate. Kahn [15] has shown that anchoring is very strong between LCs and SiO_2 or ITO.

2.1.3. *Filling the LC in the holes*

Because the LC is viscous in the nematic phase, but less viscous in the isotropic phase, we heated the LC to the isotropic phase for filling the cavities. The LC used was ZLI-2806 (LC mixture from Merck); the dielectric constant $\Delta\varepsilon$ is -4.8.

2.1.4. *Completing the cell*

To form closed cavities, the DMOAP-coated smooth plate was used to cover the top of the cavity plate. Then the temperature was lowered to form the nematic phase and align it in the holes. Next, we used glue to seal the cell and connected conducting wires onto the ITO of the two substrates. No additional spacers were provided between the SiO_2 substrate and the planar substrate. Experimentally, the space between the SiO_2 substrate and the planar substrate derives from the assembly process. Eventually it will be controlled using better assembly technology. Other cavity geometry and special design features can be incorporated for larger aperture ratios.

2.2. *Microscopic observations and measurements*

We used a Leitz polarizing microscope and crossed polarizers to observe the optical patterns from the top view of the display [7]. There is a very dark field of view with no applied voltage. When the applied voltage is a little greater than the threshold voltage, the pattern of each cavity begins to develop with a circular dark region in the centre and four petal-shaped bright regions around the circumference. If the applied voltage is increased continuously, the circular dark region shrinks and the four bright regions become brighter and expand inwards to the centre. The circular dark region finally shrinks to a central point and four dark brushes gradually become apparent. The directions of the dark brushes are always coincident with the directions of the polarizers. The electro-optical properties were measured by the LCD evaluation system LCD5100 made by Otsuka.

3. Theory

Consider a conic CCLCD with a given array of conic cylinders of LC as shown in figure 2. The thickness of the conic cylinders is D, and the radii of upper and lower circles are R_U and R_L, respectively. In the conic CCLCD, the LC molecules are perpendicularly anchored on the walls by the surfactant. The boundary conditions of the LC directors are that **n** is vertically aligned on the cylinder walls. The electrodes are located on the upper plane $z = D$ and the lower plane $z = 0$, in which the voltage V_0 is applied. The boundary conditions of the electric potential are $V(z = 0) = 0$, $V(z = D) = V_0$, and $V(z \to \infty) = 0$.

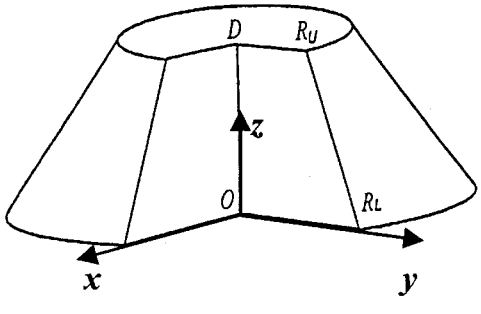

Figure 2. A local right-handed coordinate system x, y, and z of a conic CCLCD. The thickness of the conic cylinders is D, and the radii of the upper and lower circles are R_U and R_L, respectively.

The stable director field is the result of the distribution of n_1, n_2, n_3, and V that make the free energy F_g minimal. The master equations to minimize the tensor formulation of the free energy are in the appendix: equations (A7)–(A10).

We use the extended Jones matrix (EJM) method, which covers large incident angles and arbitrary orientations. It should be noted that, from an electromagnetic wave point of view, the EJM method is only allowed for the calculation of light propagation in stratified, anisotropic, inhomogeneous media. The distribution of the optical axes of the conic CCLCD is inhomogeneous, but it is not stratified. Therefore, we modified the EJM method to deal with the light propagation in the CCLCD. The detailed calculation is expressed in the appendix (optical simulation).

4. Results and discussions

4.1. *Stable structure*

To simplify the analysis, the aspect ratio of the conic cylinder is 9, the thickness $D = 5\,\mu m$ and the radii R_L and R_U are 50 and 45 μm, respectively. The material parameters used in solving the director field are $K = 13.5$ pN and $\Delta\varepsilon = -4.8$. We use the finite difference method (FDM) to solve the master equations (A7)–(A10) in the appendix, together with the boundary conditions. At the moment an analytical solution does not exist; only numerical solutions are available. The start of the numerical analysis is to discretize the problem. Because the master equations are expressed in Cartesian coordinates, we generate the grids by cubic meshes. In each grid there are n_1, n_2, n_3, and V to satisfy the master equations. The algorithm we adopt to solve the equations is the relaxation method. Next we give initial conditions for the director field and electric potential to start the calculation. We give three kinds of initial conditions that are hyperbolic, radial, and umbilic structures. These initial states all match the boundary conditions of the conic CCLCD. We find that the initial structure is still preserved under the threshold voltage, but if the applied voltage is larger than the threshold voltage, the most central region of stable structure is always the umbilic structure no matter what the initial condition was. The schematic of the director should be umbilic as shown in figure 3, and it is obvious that there is a central symmetric structure and no disclination or singularity present.

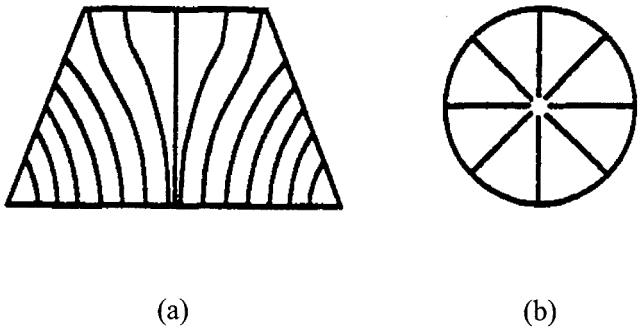

Figure 3. Schematic of the normal umbilical structure: (*a*) side view, (*b*) top view.

4.2. *Electro-optical properties*

In optical simulation, we choose the wavelength of the incident light to be 550 nm. The birefringence of the liquid crystal is $\Delta n = 0.0437$ and the refractive indices n_e and n_o are 1.5183 and 1.4746, respectively. As mentioned above, we set perpendicular alignment of the directors as the boundary conditions and an umbilic configuration as the initial condition. Then we calculate the stable state of the director field under the circumstance that no voltage is applied. The stable director field at zero-field is the initial condition of the director field when we calculate the stable director field induced by an applied voltage. As soon as the director fields are obtained, the transmittance at an applied voltage can be calculated by the optical simulation method. The dependence of transmittance on applied voltage and viewing angle will be studied, and iso-contrast contours will also be obtained. Finally, the transmittance of the conic CCLCD will be optimized by optical parameters.

4.2.1. *Azimuthal angle* $\phi = 0°$

The director of the conic CCLCD is a centrally symmetric structure. This symmetry will never appear as the optical pattern of a conic CCLCD, when the conic CCLC is between crossed polarizers. We define that the direction of the azimuthal angle $\phi = 0°$ of the conic CCLCD is the transmission axis of the polarizer. The simulation result for the threshold voltage is 1.9 V, which is coincident with the experimental result. Figure 4 shows the simulation and experimental results for the θ–T (viewing angle–transmittance) curves at different voltages V, but fixed $\phi = 0°$. The transmittance increases as the applied voltage increases; hence there is no grey-scale inversion in this azimuthal angle. Ideal polarizers are assumed in the simulation; hence the dark state in the simulation is much better than that found experimentally.

It is a reasonable assumption that the director field is cylindrically symmetric if the symmetry of the boundary

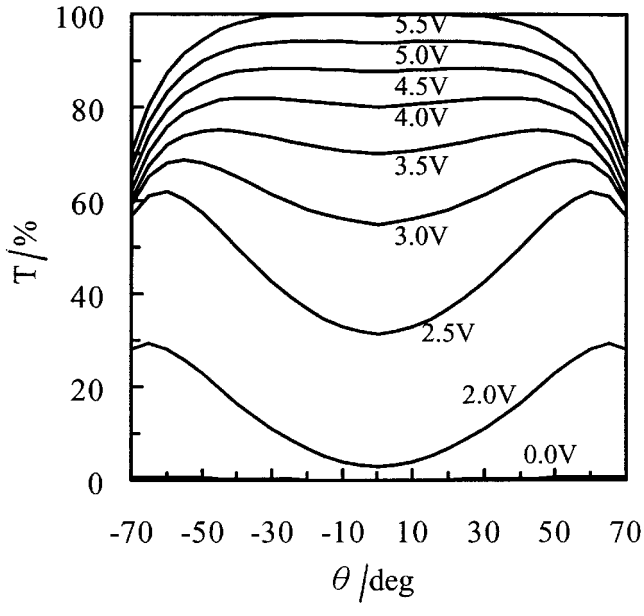

(*a*)

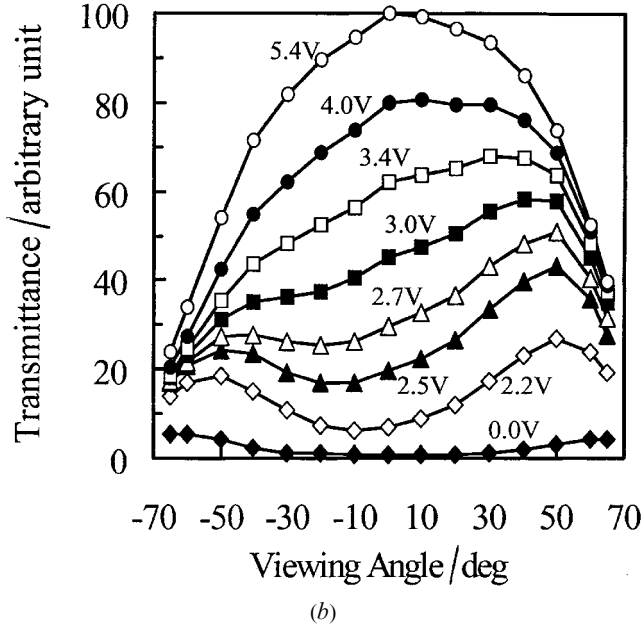

(*b*)

Figure 4. (*a*) Simulation results and (*b*) experimental results for the viewing angle-dependent normalized transmittance (T) at azimuthal angle $\phi = 0°$.

conditions is cylindrical. Therefore, in the simulation results, the transmittance curves are symmetric with respect to $\phi = 0°$. However in the experimental results, we cannot find symmetry in the grey levels. The asymmetry of transmittance is caused by the asymmetric alignment of the director field in the conic CCLC. We believe the preparation processes disturb the symmetry of the boundary conditions.

4.2.2. *Azimuthal angle* $\phi = 45°$

When fixed at $\phi = 45°$, figure 5 shows the simulation and experimental results of θ–T (viewing angle–transmittance) curves at different voltages V. The transmittance increases as the applied voltage increases. The maximal transmittance at different viewing angles decreases as the viewing angle increases at higher applied voltages. When $V < V_{th}$, transmittance increases as the viewing angle. This is due to light leakage [16] and will occur with crossed polarizers at $\phi = 45°$. This will be improved by adding a c-plate compensation film. It is obvious that the simulation and experimental results are similar.

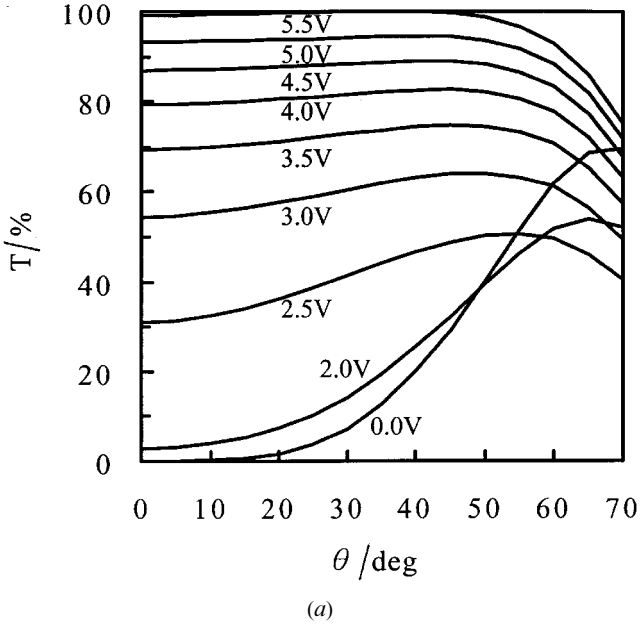

(*a*)

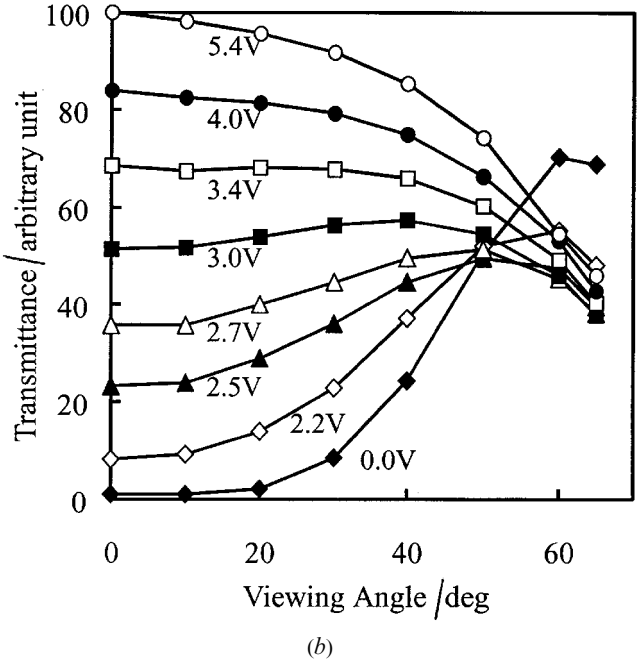

(*b*)

Figure 5. (*a*) Simulation results and (*b*) experimental results for the viewing angle-dependent normalized transmittance (T) at azimuthal angle $\phi = 45°$.

4.2.3. *Iso-contrast*

The contrast is the ratio (CR) of transmittance between the bright state and the dark state. In conic CCLCDs, the dark state is at a voltage smaller than the threshold and the bright state is at a higher voltage. Figure 6 shows the iso-contrast contours obtained from simulations and experiments in which the applied voltages are 0 V for the dark state and 5.0 V for the bright state. The iso-contrast contours can demonstrate the angular viewing capabilities. In general, the contour with $CR = 10$ limits the viewing angle of the display. Furthermore the maximal contrast has an effect on the image quality. The dark state of a conic CCLCD is almost like a homeotropic aligned LCD except for those directors near the side wall. It is well known of course that the homeotropic aligned LC has a very perfect dark state between crossed polarizers. The contour with $CR = 10$ extends to 70° on the left, right, upper, and lower sides. It is obvious that the symmetry of the simulation results is different from that of the experimental results. The reasons are the same as those mentioned above and based upon the non-uniformity of the cell gap. If the treatment of the boundary conditions is improved experimentally, the contours will be symmetric. There is degradation of the contrast ratio in terms of the azimuthal angle ($\phi = 45°$, 135°, 255°, 315°), which is verified as being due to restrictions in the characteristics of the crossed polarizers.

4.2.4. *Dependence of transmittance and contrast ratio on optical parameters*

In order to obtain more detailed optical properties of conic CCLCDs, we simulated the dependence of transmittance (T) and contrast ratio (CR) on the optical parameter ($\Delta nd/\lambda$) of the LC, where $\Delta n = n_e - n_o$ and n_e is the maximum refractive index of the extraordinary ray. We find that the dependences of T on $\Delta nd/\lambda$ are similar at $\phi = 45°$ and $\phi = 0°$, when $V = 5$ V. Figure 7 (*a*) shows the dependence of transmittance on optical parameter $\Delta nd/\lambda$ at $\phi = 45°$. Apparently, both the regions $0.6 \leqslant \Delta nd/\lambda \leqslant 0.66$ and $1.6 \leqslant \Delta nd/\lambda \leqslant 1.93$ are good choices. The latter has higher light transmittance than the former in the bright state, while the former is better in the dark state and in contrast ratio. When $\phi = 0°$ and $\Delta nd/\lambda \leqslant 1.6$, the viewing angle ($CR > 10$) is larger than 70°. This results from the good dark state where the LC

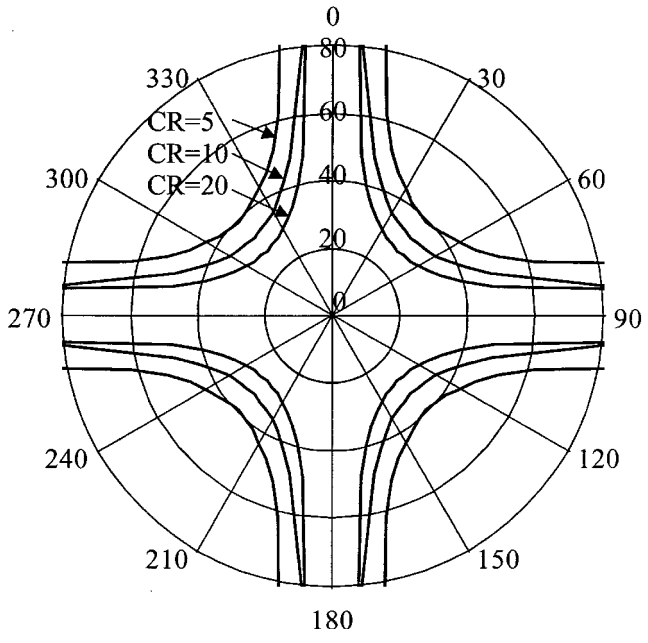

(*a*)

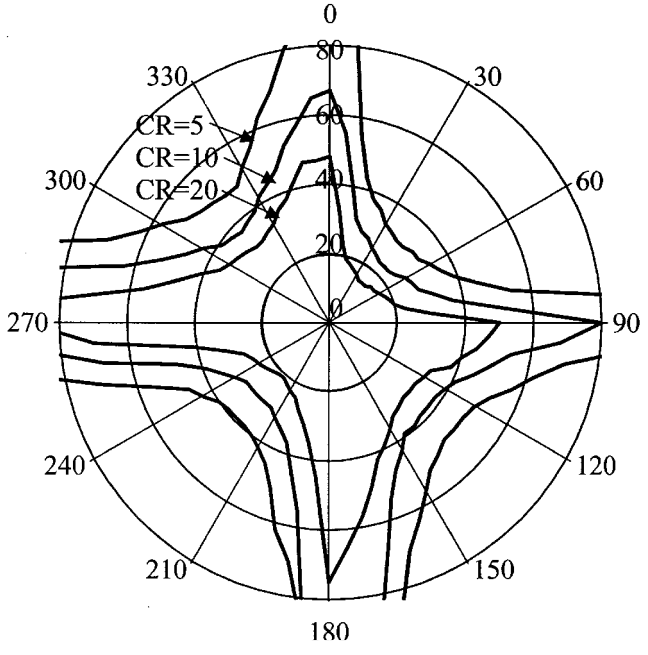

(*b*)

Figure 6. (*a*) Simulation results and (*b*) experimental results for iso-contrast ratio contours, where 0 V was used for the dark state and 5.0 V for the bright state.

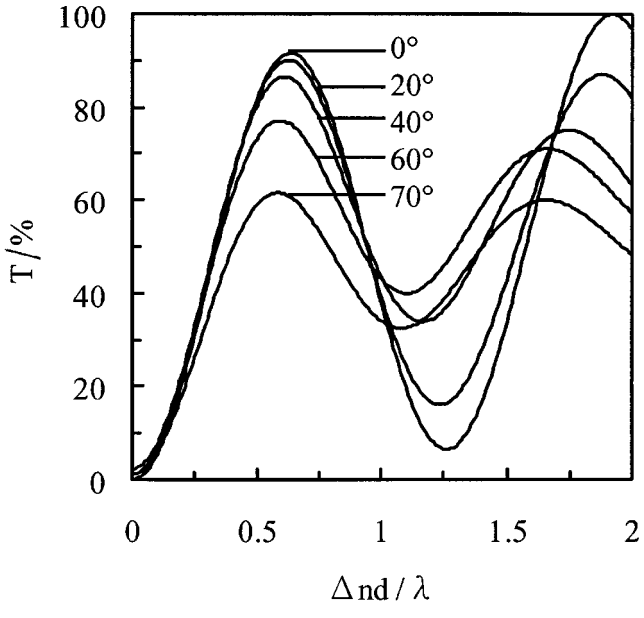

(*a*)

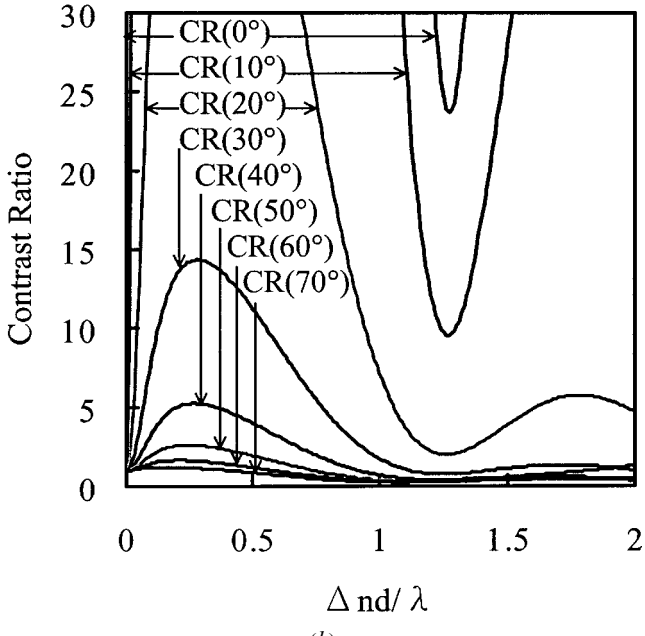

(*b*)

Figure 7. The viewing angle dependence of (*a*) $\Delta nd/\lambda$-transmittance and (*b*) $\Delta nd/\lambda$-contrast ratio at azimuthal angle $\phi = 45°$.

molecules are perpendicular to the boundary and the azimuthal angle $\phi = 0°$ is parallel to the polarizer between crossed polarizers. Figure 7(*b*) shows the dependence of *CR* on $\Delta nd/\lambda$ at $\phi = 45°$. It is obvious that the viewing angle is not good because there is light leakage in the dark state when $\phi = 45°$ with crossed polarizers.

4.2.5. *Adding a compensator*

It is well known that adding a compensator to the LCD will increase the viewing angle. For example, if we want to improve the overall viewing angle, we choose the $\Delta nd/\lambda$ of the LC to be 0.6, and then add a *c*-plate compensator of which the optical parameter $\Delta nd/\lambda$ is negative (we put it about -0.36) between the polarizer

and conic CCLC. The final iso-contrast contour is shown in figure 8. It is obvious that the viewing angle is improved.

4.3. *Comparison with four-domain VAN and four-domain twisted VAN devices*

4.3.1. *Voltage–transmittance curve*

A simple one-dimensional director field calculation for these devices and summation of the optical behaviour of CCLC and 4-D VAN devices are obtained by using Wang's LCD simulator of the National Chiao Tung University (NCTU), Taiwan. The voltage–transmittance curve is shown in figure 9. The threshold voltage of the CCLCD is the same as that of the 4-D VAN. The bright state of the CCLCD is one half of that of 4-D VAN in theory. This is because the director configuration is circularly symmetric, while the polarizers are crossed. If the incident light is circularly polarized, the bright state of the CCLCD will be increased. Besides it is an ideal condition that the 4-D VAN is aligned such that the optic axis of each domain is switched to be at 45° to the crossed polarizers. We predict that the bright state of the CCLCD is in fact larger than one half of that of the 4-D VAN.

4.3.2. *Off-axis colour shift*

We define the off-axis colour shift as the distance from the viewing angle θ to $\theta = 0$ for normal incidence in the chromaticity diagram. In order to study the off-axis colour shift (i.e. colour coordinate change as a function of θ) of the CCLCD, we employed the backlight for a typical LCD monitor (CCFL, cold cathode fluorescent lamp). Because the wavelength of the maximum brightness of a CCFL is 545 nm, Δnd can be calculated as 348.8 nm for maximum transmittance at normal incidence from figure 7(*a*). To keep Δnd constant at 348.8 nm, the dependence of transmittance on wavelength for different viewing angles θ can be obtained in figure 7(*a*). Therefore, the coordinate of the chromaticity diagram (x, y) and the off-axis colour shifts were also calculated at different viewing angles. The results for the colour shifts for $\phi = 45°$ and $\phi = 0°$ are shown in figures 10(*a*) and 10(*b*), respectively.

Next, the coordinates of the chromaticity diagram (x, y) were calculated at different viewing angles for the 4-D VAN, and 4-D twisted VAN using LCD Master of the Shintek Corp. The backlight, polarizers and parameters of the LC in the 4-D VAN and 4-D TVAN devices are the same as those for the CCLCD. The off-axis colour shifts of 4-D VAN and 4-D TVAN were also calculated at different viewing angles. The result for the colour shift are shown in figure 10. It is obvious that the off-axis colour shift for the CCLC is much less than that for the 4-D VAN and 4-D TVAN at higher viewing angles (θ larger than 30°). When θ is less than 30°, there are similar colour shifts in the three LCD modes. It is also shown that the 4-D VAN has a larger off-axis colour shift than the 4-D TVAN for $\phi = 45°$ in figure 10(*a*). However, the 4-D VAN shows the same off-axis colour shift as the 4-D TVAN for $\phi = 0°$ in figure 10(*b*).

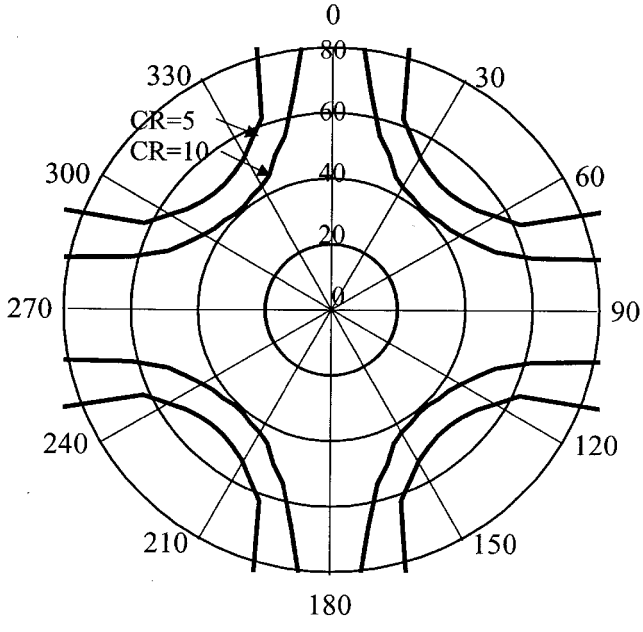

Figure 8. Simulation results of iso-contrast ratio contours for the conic CCLCD with a *c*-plate compensator, where 0 V was used for the dark state and 5.0 V for the bright state.

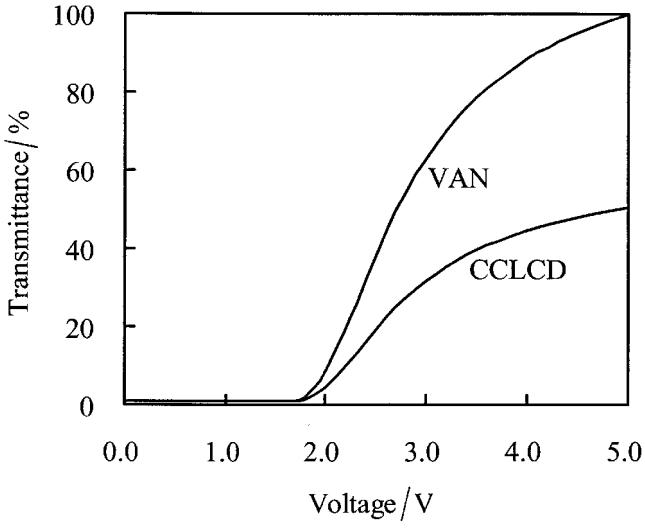

Figure 9. Voltage–transmittance curve for the CCLCD and the 4-D VAN device at normal incidence.

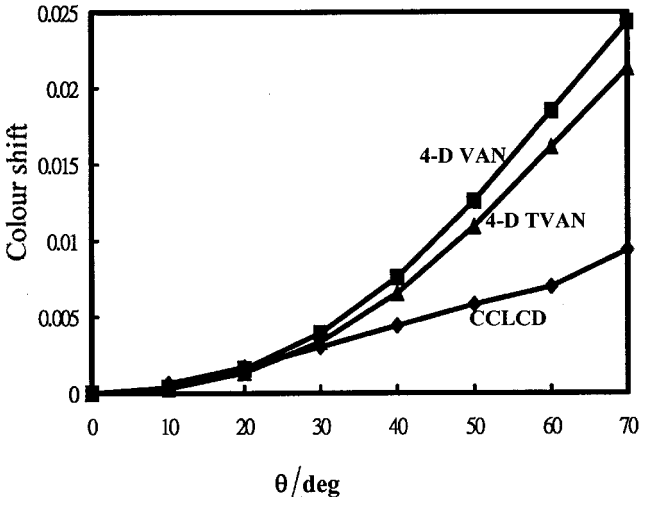

(*a*)

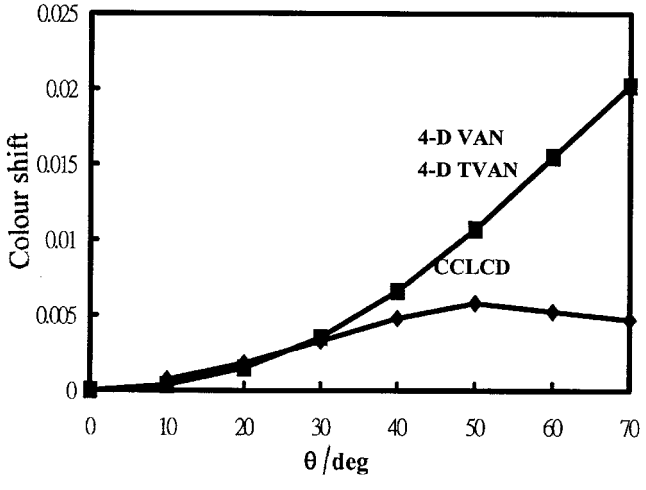

(*b*)

Figure 10. Off-axis colour shift (i.e. colour coordinate change as a function of θ) for the CCLC, 4-D VAN device, and 4-D twisted VAN device for (*a*) $\phi = 45°$ and (*b*) $\phi = 0°$.

5. Conclusion

In conclusion, conic CCLCD with wide viewing angle have been demonstrated by simulation and by experiment. The simulation of director distribution was based on the tensor form formulation of the free energy density. The simulation of the optical propagation and the calculation of the optical transmittance were based on the extended Jones matrix method. We have described the fabrication process, microscopic observations and optical measurements for conic CCLCD in detail. The viewing angle is about $\pm 70°$ for contrast ratios larger than ten in both the horizontal and vertical directions, and absence of grey-scale inversion has been demonstrated. Also, we have studied the dependence of transmittance and contrast ratio on optical parameters. Finally, we added a *c*-plate compensator to a conic CCLCD, and it was obvious that the viewing angle was improved. The off-axis colour shift has also been studied, and that for the CCLCD is less than those for 4-D VAN and 4-D twisted VAN devices.

This research was supported in part by the Chinese National Science Council under Contract No. NSC 89-2112-M-035-00 7 and the Electronics Research & Service Organization of the Industrial Technology Research Institute, Taiwan, ROC. The authors also acknowledge the Nano Device Laboratory, Taiwan, ROC. We are indebted to Prof. J. J. Wu of the Department of Physics, Soochow University, Taipei, and Dr C.-K. Wei of the Chi Mei Optoelectronic Corporation, Tainan, Taiwan, ROC, for useful discussions.

Appendix

Consider a conic CCLCD with a given array of conic cylinders of the LC as shown in figure 2. The thickness of the conic cylinder cylinders is D and the radii of upper and lower circles are R_U and R_L, respectively. In the conic CCLCD, the LC molecules are perpendicularly anchored on the walls by the surfactant. The boundary conditions of the LC directors are that **n** is vertically aligned on the cylinder walls. The electrodes are located on the upper plane $z = D$ and the lower plane $z = 0$, in which the voltage V_0 is applied. The boundary conditions of the electric potential are $V(z = 0) = 0$, $V(z = D) = V_0$, and $V(z \to \propto) = 0$.

Director modelling

The tensor formulation of the deformation energy density, F_s, expressed by Cartesian coordinates is

$$F_s = \frac{K}{4} Q_{jk,l} Q_{jk,l}, \quad i,j,k,l = 1,2,3 \tag{A1}$$

$$Q_{ij} = \frac{1}{2} Q(3n_i n_j - \delta_{ij}) \tag{A2}$$

$$Q_{ij,l} = \frac{\partial Q_{ij}}{\partial x_1}, \quad x_1 = x, x_2 = y, x_3 = z \tag{A3}$$

where K is the approximated Frank elastic constant, and Q_{ij} is the element of the order parameter tensor of the LC. In tensor calculus, it is quite advantageous to make use of the Einstein summation convention, i.e. $A_i B_i = A_1 B_1 + A_2 B_2 + A_3 B_3$. The symbol δ_{ij} is the Kronecker delta, which is defined as

$$\delta_{ij} = \begin{cases} 0, & \text{if } i = j \\ 1, & \text{if } i \neq j \end{cases}.$$

The coupling between the electric field and director field gives rise to a free energy density

$$F_e = \frac{1}{2}\varepsilon_0 \varepsilon_{jk} V_{,j} V_{,k} + \frac{1}{2}\varepsilon_0 \Delta\varepsilon V_{,j} V_{,k} Q_{jk}, \quad i, j, k = 1, 2, 3 \tag{A4}$$

$$V_{,j} = \frac{\partial V}{\partial x_j} \tag{A5}$$

where ε_{jk} corresponds to the element of the relative permittivity tensor, $\Delta\varepsilon$ denotes the dielectric anisotropy, and V is the electric potential. The free energy density of the LC is

$$F_g = F_s - F_e. \tag{A6}$$

The stable director field is the result of the distribution of n_1, n_2, n_3, and V that make the free energy F_g minimal. The master equations to minimize the free energy can be obtained by using the variation method as follows.

$$\frac{\partial F_g}{\partial n_1} - \frac{d}{dx_1}\left(\frac{\partial F_g}{\partial n_{1,x_1}}\right) - \frac{d}{dx_2}\left(\frac{\partial F_g}{\partial n_{1,x_2}}\right) - \frac{d}{dx_3}\left(\frac{\partial F_g}{\partial n_{1,x_3}}\right) = 0 \tag{A7}$$

$$\frac{\partial F_g}{\partial n_2} - \frac{d}{dx_1}\left(\frac{\partial F_g}{\partial n_{2,x_1}}\right) - \frac{d}{dx_2}\left(\frac{\partial F_g}{\partial n_{2,x_2}}\right) - \frac{d}{dx_3}\left(\frac{\partial F_g}{\partial n_{2,x_3}}\right) = 0 \tag{A8}$$

$$\frac{\partial F_g}{\partial n_3} - \frac{d}{dx_1}\left(\frac{\partial F_g}{\partial n_{3,x_1}}\right) - \frac{d}{dx_2}\left(\frac{\partial F_g}{\partial n_{3,x_2}}\right) - \frac{d}{dx_3}\left(\frac{\partial F_g}{\partial n_{3,x_3}}\right) = 0 \tag{A9}$$

$$\mathrm{div}[\varepsilon_0 \varepsilon_{jk} (\nabla V)_k]_j = 0. \tag{A10}$$

Optical simulation

We use the extended Jones matrix (EJM) method, which covers large incident angles and arbitrary orientations. This method is simpler than the 4×4-matrix method and thus requires less computation time. It should be noted here that, from an electromagnetic wave point of view, the EJM method is only allowed for the calculation of light propagation in stratified, anisotropic, inhomogeneous media. However, because the distribution of the optical axes of the conic CCLCD is inhomogeneous, but not stratified, we modified the EJM method to deal with the light propagation in a CCLCD. The optical behaviour of a CCLCD is modelled by dividing the material into an array of CCLC [17]. The column is parallel to the incident ray passing into the LC and the sublayers in column lie parallel to the substrate. Each element is assumed to have uniaixal birefringence, with a uniform optic axial direction. The optic axes of each element can be interpolated by results from the front sections and vary from element to element. Because the molecular director of the LC is continuous, the change in refractive index is small; we assume that the light will not refract outside the primary column. The passage of light through each column of cells is considered in turn; the transmittance of each column is calculated by the EJM method and the total transmittance of the CCLCD is the summation of all the columns.

Consider a column with N sublayers; in each sublayer, the medium is assumed to be uniaxial and homogeneous, but the orientations of the optic axis are different. For a given incident electric field (A_s, A_p), the transmitted electric field (A'_s, A'_p) can be calculated by

$$\begin{bmatrix} A_s \\ A_p \end{bmatrix} = \boldsymbol{M}_A \boldsymbol{M}_{LC} \boldsymbol{M}_P \begin{bmatrix} A_s \\ A_p \end{bmatrix}$$

$$\boldsymbol{M}_{LC} = D_{Ag} P_N D_{N-1,N} P_{N-1} D_{N-2,N-1} \cdots D_{2,3} P_2 D_{1,2} P_1 D_{Pg},$$

$$D_{j,j+1} = \begin{bmatrix} \hat{o}_j & \hat{o}_{j+1} & \hat{e}_j & \hat{o}_{j+1} \\ \hat{o}_j & \hat{e}_{j+1} & \hat{e}_j & \hat{e}_{j+1} \end{bmatrix}$$

where $D_{j,j+1}$ is the dynamic matrix between the jth and $(j+1)$th sublayers, and P_j is the transfer matrix of the jth sublayer. The unit vectors of the eigen-modes, $\hat{o}$ and $\hat{e}$, in each sublayer are given by

$$\hat{o} = \frac{\hat{c} \times \bar{k}_o}{|\hat{c} \times \bar{k}_o|}; \quad \hat{e} = \frac{\bar{k}_o \times \hat{o}}{|\bar{k}_o \times \hat{o}|}.$$

The $\boldsymbol{M}_A$ and $\boldsymbol{M}_P$ are matrices of analyser and polarizer, respectively. They can be expressed as

$$\boldsymbol{M}_A = \begin{bmatrix} \hat{a}_t & \hat{s} & \hat{a}_a & \hat{s} \\ \hat{a}_t & \hat{p} & \hat{a}_a & \hat{p} \end{bmatrix} \begin{bmatrix} 1 & 0 \\ 0 & 0 \end{bmatrix} \begin{bmatrix} \hat{s} & \hat{a}_t & \hat{p} & \hat{a}_t \\ \hat{s} & \hat{a}_a & \hat{p} & \hat{a}_a \end{bmatrix}$$

$$\boldsymbol{M}_P = \begin{bmatrix} \hat{p}_t & \hat{s} & \hat{p}_a & \hat{s} \\ \hat{p}_t & \hat{p} & \hat{p}_a & \hat{p} \end{bmatrix} \begin{bmatrix} 1 & 0 \\ 0 & 0 \end{bmatrix} \begin{bmatrix} \hat{s} & \hat{p}_t & \hat{p} & \hat{p}_t \\ \hat{s} & \hat{p}_a & \hat{p} & \hat{p}_a \end{bmatrix}$$

where $\hat{p}_t$, $\hat{p}_a$, $\hat{a}_t$, $\hat{a}_a$ are unit vectors of the transmission axis of the polarizer, the absorption axis of the polarizer, the transmission axis of the analyser, and the absorption axis of the analyser, respectively. Analogously to the unit vectors of eigen-modes, these unit vectors are given by

$$\hat{p}_t = \frac{\hat{c} \times \bar{k}_i}{|\hat{c} \times \bar{k}_i|}; \quad \hat{p}_a = \frac{\bar{k}_i \times \hat{p}_t}{|\bar{k}_i \times \hat{p}_t|}$$

$$\hat{a}_t = \frac{\hat{c} \times \bar{k}_i}{|\hat{c} \times \bar{k}_i|}; \quad \hat{a}_a = \frac{\bar{k}_i \times \hat{a}_t}{|\bar{k}_i \times \hat{a}_t|}$$

where $\hat{c}$ and $\bar{k}_i$ are the optic axes of the polarizer (or analyzer) and the wave vector of the incident light, respectively. Also $\hat{p}$ and $\hat{s}$ are the unit vectors of the p-polarization and s-polarization of the incident light, respectively.

References

[1] Yang, Y. H., 1991, *Proc. IDRC'91*, 68.
[2] Ohmuro, K., Kataoka, S., Sasaki, T., and Koike, Y., 1997, *SID'97 Dig*., 845.
[3] Yamada, N., Kohzaki, S., Funada, F., and Awane, K., 1995, *SID'95 Dig*., 575.
[4] Kuo, C.-L., Miyashita, T., Suzuki, M., and Uchida, T., 1996, *Appl. Phys. Lett*., **68,** 1461.
[5] Vithana, H., Fung, Y. K., Jamal, S. H., Herke, R., Bos, P. S., and Johnson, D. L., 1995, *SID'95 Dig*., 873.
[6] Bos, P. J., Vithana, H. K., Johnson, D. L., and Chen, J., 2000, U.S. Patent 6 141 074.
[7] Liang, B.-J., Chen, S.-H., and Wang, Y. F., 1998, *Appl. Phys. Lett*., **72,** 1290.
[8] Liang, B.-J., Chen, S.-H., Wu, C.-R., Wei, C.-K., and Kuo, C.-L., 1998, in Proceedings of SPIE Conference on Display Technologies, Vol. II, pp. 215–222.
[9] Liang, B.-J., Chen, S.-H., Wu, C.-R., Wei, C.-K., and Kuo, C.-L., 1999, U.S. Patent 5 978 062.
[10] Wei, J.-G., and Chen, S.-H., 1994, *Jpn. J. appl. Phys. 2*, **33,** L660.
[11] Wei, J.-G., and Chen, S.-H., 1994, *Jpn. J. appl. Phys. 1*, **33,** 6249.
[12] Schiele, K., and Trimper, S., 1983, *Phys. Stat. Sol*., **118,** 267.
[13] Mori, H., Gartland, E. C., Kelly, J. R., and Bos, P. J., 1999, *Jpn. J. appl. Phys. 1*, **38,** 135.
[14] Gu, C., and Yeh, P., 1993, *J. opt. Soc. Am*., **A10,** 996.
[15] Kahn, F. J., 1973, *Appl. Phys. Lett*., **22,** 386.
[16] Herke, R., Jamal, S. H., and Kelly, J. R., 1995, *J. SID*, **3,** 9.
[17] Nichlson, T. M., 1989, *Mol. Cryst. liq. Cryst*., **177,** 163.